

Printable Polar Silicone Elastomers for Healable Supercapacitive Strain Sensors

Journal Article**Author(s):**

von Szczepanski, Johannes; Roels, Ellen; Siqueira, Gilberto; Danner, Patrick M.; Wolf, Jana; Legrand, Julie; Brancart, Joost; Terryn, Seppe; van Assche, Guy; Vanderborght, Bram; Opris, Dorina M.

Publication date:

2023-12-21

Permanent link:

<https://doi.org/10.3929/ethz-b-000644114>

Rights / license:

[Creative Commons Attribution-NonCommercial 4.0 International](#)

Originally published in:

Advanced Materials Technologies 8(24), <https://doi.org/10.1002/admt.202301310>

Printable Polar Silicone Elastomers for Healable Supercapacitive Strain Sensors

Johannes von Szczepanski, Ellen Roels, Gilberto Siqueira, Patrick M. Danner, Jana Wolf, Julie Legrand, Joost Brancart, Seppe Terryn, Guy van Assche, Bram Vanderborght, and Dorina M. Opris*

Soft strain sensors with high sensitivity and the ability to recover from damages are required in the emerging field of self-healing soft robotics. Herein, printable supercapacitive strain sensors that can heal upon moderate heating (75 °C for 10 min) and exhibit a 30 times higher sensitivity than PDMS-based sensors are developed. For the sensor's core layer and electrode, a nitrile-functional polysiloxane that contains an active ionic initiator and can heal by siloxane equilibration at elevated temperatures is used.

Supercapacitive strain sensors prepared from the elastomer are highly sensitive at low strains of 0–30%, enabled by the electric double-layer formation of the ionic initiator. After healing, the sensors exhibit nearly unaltered performance in tensile testing. Due to the thermoreversible nature of the elastomer network, patterned core layers with different microstructures can be printed by direct ink writing. The capacitive sensors based on these microstructured films reach a higher sensitivity and linearity than those based on unstructured films. Finally, the sensor is integrated into a soft robotic finger and the sensor's ability to determine the bending angle is validated by motion capture. This technology can provide new opportunities to equip soft robotic devices with custom-printed, healable strain sensors.

simple structure and low power consumption, combined with low hysteresis and high linearity.^[4,5] They can be used as pressure or strain sensors in many applications, including body activity monitoring in smart wearables,^[6,7] deformation tracking in soft robotics, and tactile measurements in user interfaces.^[8,9] In soft robotic systems, capacitive strain sensors monitor and control soft robots' deformation and position. The sensitivity of capacitive strain sensors is given by the gauge factor (GF), which describes the ratio of normalized capacitance change ($\Delta C/C_0$) and strain (ϵ) (Equation 1).^[10]

$$GF = \frac{\Delta C}{C_0 \epsilon} \quad (1)$$


Soft sensors are susceptible to damage like punctation or tear caused by external sharp objects or overstretching.^[11] Therefore, developing sensors with healing ability that can recover after the damage is highly interesting. Healing

increases the lifetime of the devices and is, therefore, more sustainable in terms of material consumption.^[12] Damage recovery is especially important if the sensor is fully integrated into the body or a soft robotic device and cannot be exchanged easily. Therefore, researchers have focused on developing stretchable, capacitive sensors with intrinsic healing capability.^[13–17]

1. Introduction

In recent years, there has been an increasing demand for stretchable and soft sensors promoted by their various applications in wearable electronics and soft robotics.^[1–3] Among the different soft sensor technologies, capacitive sensors stand out by their

J. von Szczepanski, G. Siqueira, P. M. Danner, J. Wolf, D. M. Opris
Laboratory for Functional Polymers
Swiss Federal Laboratories for Materials Science and Technology (Empa)
Ueberlandstr. 129, Dübendorf 8600, Switzerland
E-mail: dorina.opris@empa.ch

 The ORCID identification number(s) for the author(s) of this article can be found under <https://doi.org/10.1002/admt.202301310>

© 2023 The Authors. Advanced Materials Technologies published by Wiley-VCH GmbH. This is an open access article under the terms of the Creative Commons Attribution-NonCommercial License, which permits use, distribution and reproduction in any medium, provided the original work is properly cited and is not used for commercial purposes.

DOI: 10.1002/admt.202301310

J. von Szczepanski, G. Siqueira, P. M. Danner, J. Wolf, D. M. Opris
Department of Materials
ETH Zurich
Vladimir-Prelog-Weg 5, Zurich 8093, Switzerland
E. Roels, J. Brancart, S. Terryn, G. van Assche
Physical Chemistry and Polymer Science (FYSC)
Vrije Universiteit Brussel (VUB)
Pleinlaan 2, Brussels 1050, Belgium
E. Roels, J. Legrand, S. Terryn, B. Vanderborght
Brubotics
Vrije Universiteit Brussel (VUB) and Imec
Pleinlaan 2, Brussels 1050, Belgium
G. Siqueira
Laboratory for Cellulose and Wood Materials
Swiss Federal Laboratories for Materials Science and Technology
Ueberlandstr. 129, Dübendorf 8600, Switzerland

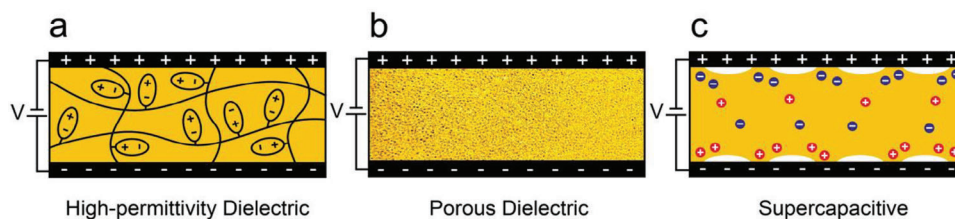


Figure 1. Three approaches for increasing the sensitivity of capacitive sensors. a) High-permittivity dielectric: deformation of a sensor with a high-permittivity dielectric gives a higher absolute change in capacitance. b) Porous dielectric: the air inside a porous dielectric is pushed out during compression, which increases permittivity upon deformation. c) Supercapacitive sensor: an electrolyte core layer containing ions is used instead of a dielectric. The ions accumulate at the interface with the electrodes and form an EDL, whose capacitance is several orders of magnitude higher than the parallel plate capacitance. Usually, a structured electrode or core layer is used to increase the change in contact area upon deformation.

Different healing mechanisms have been successfully used to obtain self-healing capacitive sensors. For instance, Zhang et al.^[15] reported a self-healing elastomer based on a combination of dynamic metal-coordinated and hydrogen bonds. A self-healable conductive layer was obtained by filling the elastomer with silver flakes. The combination of the two materials yielded stretchable capacitive pressure sensors. However, the healing process took 48 h at room temperature.^[15] Additionally, the sensor characterization was purely qualitative. Faster healing sensors were explored by Ling et al.,^[16] who developed a nanocomposite based on polyurethane and reduced graphene oxide/carbon nanotubes. The elastomer can heal upon heating to 100 °C for 10 min, which is enabled by disulfide bonds in the polyurethane backbone and hydrogen bonds. The capacitive strain sensors performed similarly in the pristine state and after healing. However, the sensors' sensitivity was low, with a GF of only 0.45.^[16] Rao et al.^[17] reported a self-healing capacitive strain sensor based on polydiacetylene-polyacrylic acid-hydrogel. The self-healing is enabled by electrostatic interactions between carboxylate groups and Cr³⁺ ions. They achieved a high stretchability of 500% combined with a large GF of up to 160, which was reached due to the electrical double-layer formation of the Cr³⁺ ions.^[17] However, hydrogel-based sensors are usually temperature or humidity-sensitive, which affects the sensors' accuracy.^[5,18]

Besides the interest in healing ability, capacitive sensors also need improvement in terms of sensitivity and linearity of the response.^[19–21] A first approach to increase the sensitivity is by increasing the relative permittivity of the dielectric (Figure 1a).^[22,23] A high-permittivity dielectric increases the capacitance of the parallel-plate capacitor and leads to a larger absolute change in capacitance upon deformation. A second approach is the application of a porous dielectric layer (Figure 1b). The air inside the dielectric layer is pressed out during deformation, which leads to an increase in permittivity, and therefore, a larger relative change in capacitance.^[5] Porous dielectrics can be easily fabricated, for example, by adding sugar crystals to the dielectric matrix and later dissolving the sugar in water.^[24] However, most methods do not allow good control over the size and spatial distribution of the pores.^[25] A third approach to increasing the sensitivity of capacitive sensors is the so-called supercapacitive sensors.^[26,27] Ions are introduced into the core layer, which typically consists of hydrogels.^[5] When a voltage is applied, these ions form an electric double layer (EDL) at the interface with the electrodes (Figure 1c).^[28] The EDL capacitance is several orders of magnitude larger than the one of the parallel plate capacitor, which leads

to a huge increase in sensitivity.^[29] The sensitivity can be further enhanced by introducing a microstructure, such as pyramids or hemispheres, to the electrode or core layer.^[30–32] In this case, the change in the contact area between the electrode and core layer upon deformation is drastically increased.

In this work, we synthesize a polysiloxane elastomer with polar cyanopropyl side groups and an active ionic initiator and use it to build supercapacitive strain sensors that can heal after damage. The ionic initiator, TMAH, contributes to an increase in the sensitivity of the sensors by forming an EDL at the electrode interface. The rheological and thermoreversible properties of the elastomer allowed us to print microstructured sensor core layers by direct ink writing (DIW). The printed sensors show increased sensitivity compared to isotropic, melt-pressed sensors, which can be attributed to the structured interface. Finally, we prove that our sensor can be used to measure the bending movement of a soft robotic finger. In the future, our elastomers could be used to print customized sensors for wearable electronics or motion sensors for healable soft robots.

2. Elastomer Synthesis and Characterization

Two materials are needed for supercapacitive strain sensors: a stretchable elastomer core layer and a stretchable conductive material, which serves as electrodes. Both materials must heal under similar conditions to obtain an integrally healable sensor. Therefore, we developed a healable silicone elastomer containing an ionic initiator that can be filled with carbon black to serve as electrode material.

Silicone elastomers with active chain end, synthesized by anionic ring-opening polymerization, can heal by equilibration between the cross-linked network and low molar mass cycles upon heating. This process is known as siloxane equilibration.^[33] The silanolate end groups of the silicone backbone remain active in the cross-linked network and can backbite and cleave the chains to form low molar mass fragments. At elevated temperatures, the backbiting is favored and the equilibrium is shifted to the side of low molar mass fragments and cycles. This leads to a reversible softening of the material. The network is formed again upon cooling and the initial elastic properties are recovered. The healing temperature and time are reduced significantly by introducing polar side groups to the siloxane backbone. In previous work, we used this healing mechanism to prepare healable and recyclable artificial muscles.^[34] Polar side groups also increase the relative permittivity of the elastomer, which is beneficial for

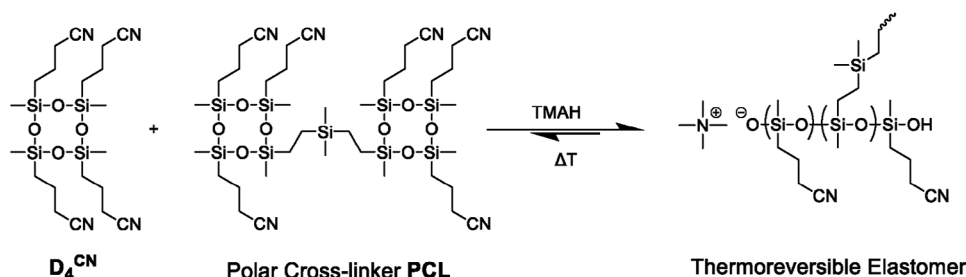


Figure 2. Synthesis of thermoreversible elastomers by anionic ring-opening polymerization of monomer D_4^{CN} and cross-linker PCL. The chain ends remain active in the product and the silanolate end groups can cleave the polymer chains through backbiting. An equilibrium between a cross-linked network and low molar mass species is formed, which can be shifted as a function of temperature.

capacitive strain sensors, as described above. We combine high-permittivity and healing ability in one elastomer by synthesizing a silicone elastomer with polar cyanopropyl groups by anionic ring-opening polymerization (Figure 2). A cyclic silicone monomer with cyanopropyl groups (D_4^{CN}) and a specially designed polar bicyclic monomer cross-linker (PCL) were first synthesized. These monomers are used in an anionic ring-opening polymerization with tetramethylammonium hydroxide (TMAH) as an initiator. Polymerization and cross-linking occur simultaneously, giving an elastomer network in one step. The matching polarities of cross-linker and monomer allow us to carry out the reaction solvent-free. This is advantageous compared to our previous work, where THF as solvent was required to avoid phase separation of the nonpolar cross-linker and the polar monomer.^[34] THF promotes backbiting during the polymerization reaction and increases the amount of cyclic byproducts.

Three elastomers (E1–E3) with different amounts of cross-linker PCL (10, 15, and 20 phr) were synthesized to optimize the mechanical properties, namely increase the elongation at break and decrease the viscous losses (Table 1). The elongation at break decreases with an increasing amount of PCL from $119 \pm 8\%$ for elastomer E1 to $43 \pm 5\%$ for elastomer E3, as is expected from the increasing cross-linking density (Figure 3a). At the same time, the modulus increases from 95 ± 7 kPa for elastomer E1 to 303 ± 49 kPa for elastomer E3. The stress–strain curves were averaged from five independent samples and the individual curves are shown in Figure S1 (Supporting Information). The dynamic mechanical analysis (DMA) curves of elastomers E1–E3 are shown in Figure 3b. For elastomers E2 and E3, low viscous losses are observed with a $\tan(\delta)$ of 0.06 ± 0.01 and 0.04 ± 0.01 at 1 Hz. Elastomer E1 shows larger viscous losses, especially at high frequencies with a $\tan(\delta)$ of 0.25 ± 0.03 at 1 Hz. In soft robotic applications, strain sensors require large elongations and low vis-

cou losses of the elastomers. Viscous losses introduce time dependencies in the sensor response, which makes the modelization and calibration of the sensors more complex. Therefore, we selected elastomer E2 for the following experiments, as it gives the best combination of properties with an elongation at break of $71 \pm 6\%$ and low viscous losses.

We examined the dielectric properties of elastomer E2 by impedance spectroscopy. The relative permittivity as a function of the frequency is shown in Figure 3c for elastomer E2 and PDMS. At 1 kHz, elastomer E2 has a relative permittivity of 19.9, which is more than 5 times higher than the relative permittivity of PDMS (3.6). A high dielectric permittivity is beneficial in capacitive sensors, as it increases the absolute change in capacitance upon deformation. A detailed dielectric characterization with permittivity, dielectric loss, loss tangent, and conductivity as a function of frequency is shown in Figure S2 (Supporting Information). Elastomer E2 exhibits a relatively high conductivity of $\approx 10^{-7}$ S cm^{-1} , due to the ionic initiator, which remains active in the product. Elastomer E2 also shows a strong increase in permittivity toward low frequencies. This effect is caused by ionic contaminants and the ionic initiator, TMAH, which accumulates at the interface with the electrode at low frequencies.

Besides the dielectric elastomer, a stretchable conductive material is needed for capacitive strain sensors. The conductive electrode material should be based on the same chemistry as elastomer E2 to ensure healing ability and good interfacial connection with elastomer E2 by covalent bonding across the interface. A stretchable electrode material was prepared by mixing 15 wt% carbon black powder with monomer D_4^{CN} and cross-linker PCL before the polymerization. A lower cross-linker concentration of 10 phr was used for the electrode to ensure sufficient elongation of the composite material. The cross-linked electrode material shows an elongation at a break of $106 \pm 3\%$ and a modulus of 428 ± 14 kPa (Figure S3a, Supporting Information; Table 1), which is higher than the modulus of the dielectric elastomer E2 of 165 ± 14 kPa. The softer nature of the dielectric elastomer E2 compared to the electrode material is beneficial to ensure compression of the core layer during deformation. The viscous losses of the electrode material are similar to elastomer E1 with a $\tan(\delta)$ of 0.25 ± 0.01 at 1 Hz (Figure S3b, Supporting Information). The resistivity of the electrode material was determined by impedance spectroscopy (Figure S4, Supporting Information). The composite shows a resistivity of 24 ± 2 k Ω cm at 1 kHz, which is sufficient for the application in capacitive sensors. The stress relaxation of elastomer E2 and the electrode material was investigated

Table 1. Composition and mechanical properties of elastomers E1–E3 and the electrode material.

Elastomer	PCL [phr]	Carbon Black [wt%]	Elongation [%]	Modulus [kPa]	$\tan(\delta)$ at 1 Hz
E1	10	–	119 ± 8	95 ± 7	0.25 ± 0.03
E2	15	–	71 ± 6	165 ± 14	0.06 ± 0.01
E3	20	–	43 ± 5	303 ± 49	0.04 ± 0.01
Electrode	10	15	106 ± 3	428 ± 14	0.25 ± 0.01

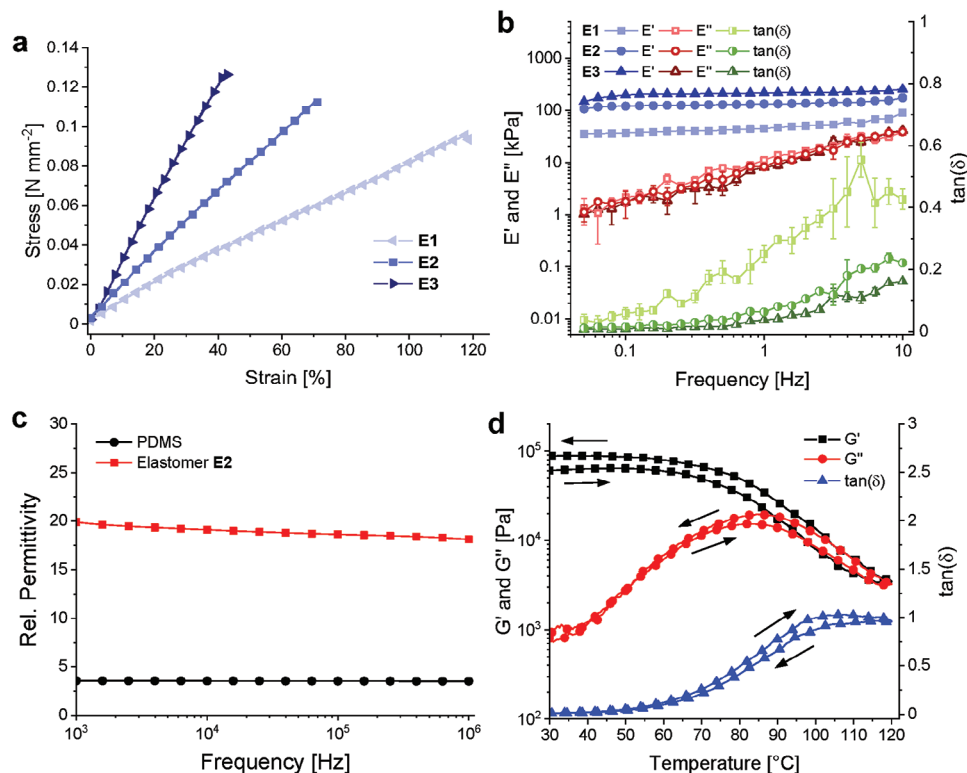


Figure 3. a) Stress–strain curves of elastomers E1–E3 with different concentrations of cross-linker PCL. The elongation at break decreases with increasing cross-linker concentration. b) DMA traces of elastomers E1–E3. The storage modulus increases with increasing cross-linker concentration, while the viscous losses decrease. If not shown, the error bars are smaller than the symbol size. c) Permittivity as a function of frequency for elastomer E2 and PDMS. The permittivity of the polar elastomer is more than five times higher than the one of PDMS. The measurement was averaged from three independent samples, error bars are smaller than the symbol size. d) Temperature-dependent shear rheology measurement of elastomer E2 proves the thermoreversible softening of the elastomer (heating and cooling rate: 1 K min⁻¹, angular frequency: 1 rad s⁻¹, strain: 0.1%).

by applying a strain of 30% and measuring the decay of the stress (Figure S5, Supporting Information). The stress relaxation is very small for elastomer E2 and more pronounced for the electrode material, which is in accordance with the viscous losses observed in the DMA measurements.

The initiator TMAH remains active in elastomer E2 and forms active silanolate chain ends. These chain ends can undergo a backbiting reaction at temperatures above 70 °C, which is facilitated by the polar cyanopropyl side groups. This backbiting leads to a partial cleavage of the polymer chains into low molar mass chain segments and cycles. Therefore, the material softens upon heating, can be (re)processed, and can heal damages. This process is attributed to the equilibration between cross-linked network and low molar mass compounds at elevated temperatures and is not a consequence of phase transition. The absence of phase transitions in the temperature range between 20 and 150 °C can be seen from the differential scanning calorimetry curve of elastomer E2, where only the T_g is visible at -55 °C (Figure S6, Supporting Information). The thermoreversible softening of elastomer E2 was proven by temperature-dependent dynamic shear rheology measurements (Figure 3d). At 30 °C, the material is in the cross-linked state and can be characterized as an elastic solid ($G' \gg G''$). When the temperature increases, the elastomer network is partially cleaved, and the material becomes softer. Above 100 °C, the material undergoes a transition into a

viscous fluid, and a crossover between G' and G'' is observed. When cooling back to 30 °C, the network is reformed and the initial mechanical properties are restored. Only the storage modulus, G' , exhibits a larger value after the heating cycle, which might be caused by partial, irreversible cross-linking of the nitrile groups at high temperatures of ≈ 120 °C. A similar thermoreversible effect was observed for the electrode material but with a less pronounced softening at elevated temperatures due to the interaction of the carbon black particles (Figure S7, Supporting Information). Therefore, the electrode material can be processed by melt pressing, but the softening effect is insufficient for printing the material by DIW. The viscous flow activation energy of the healing process can be determined from the Arrhenius plot obtained by plotting the \ln of the loss modulus, $\ln(G''')$, as a function of $1/T$ (Figure S8, Supporting Information).^[35] Classically, the zero-shear viscosity or the relaxation time is used to determine the activation energy. However, we observed a Newtonian behavior for our material in the flow curve at 120 °C (Figure S9, Supporting Information). The viscosity is independent of the shear rate. Therefore, the activation energy based on G''' measured at a shear rate of 1 rad s⁻¹ gives a reliable value for the viscous flow activation energy of our material. Multiplication of the slope of the linear regime between 90 and 115 °C of 8134 K with the gas constant, R , yields an activation energy of ≈ 68 kJ mol⁻¹. This value is lower compared to the activation

energies of other dissociative dynamic covalent networks, such as Diels–Alder-based networks with an activation energy of 88–101 kJ mol⁻¹.^[35–38] Therefore, our materials soften and heal at comparably low temperatures of 70–80 °C.

3. Capacitive Strain Sensor Performance and Healing

Soft strain sensors with healing ability are interesting for damage-resilient soft robotic devices. We built strain sensors by sandwiching a melt-pressed film of elastomer **E2** with a thickness of ≈ 300 μm between two films of electrode material with a thickness of ≈ 300 μm and heating to 70 °C for 5 min. Dielectric and electrode materials are based on the same thermoreversible chemistry. The active silanolate end groups can backbite and cleave the network, which is favored at elevated temperatures, thus shifting the equilibrium to the side of low molar mass fragments. Upon cooling, new covalent bonds are formed across the interface of the dielectric and electrode, as the polymer network forms again. Films of electrode and elastomer **E2** connected by this procedure exhibit excellent interfacial connection and can be stretched to 40% strain without delaminating (Figure S10, Supporting Information). In the next step, the sensor was characterized by uniaxial stretching to 30% strain while measuring the change in capacitance with an LCR meter at 1 kHz. A strain rate of 300% min⁻¹ was selected, as these fast deformations coincide with deformation rates present in soft robotics during actuation. For comparison with the sensors based on elastomer **E2**, we conducted the same uniaxial stretching experiments with sensors containing PDMS as dielectric, yet the same electrodes. The measured GF (see Equation 1) is more than 30 times higher for the sensors based on elastomer **E2** (GF = 12.7 ± 0.8) compared to the PDMS sensor (GF = 0.41 ± 0.01) (Figure 4a). A contribution of ionic conductivity most probably causes the strong capacitance change in the sensors based on elastomer **E2**.^[5] The tetramethylammonium ions of the initiator remain active in the product and are mobile in the polymer network. The difference in ionic conductivity between elastomer **E2** and PDMS can be seen in the plot of the phase angle between current and voltage as a function of the frequency (Figure S11, Supporting Information). At 1 kHz, elastomer **E2** has a phase angle close to 0°, which is characteristic of resistive behavior, while the PDMS sample shows a value close to -90°, characteristic of capacitive behavior. At a higher frequency of 10 kHz, the phase angle of elastomer **E2** decreases and at 100 kHz the phase angle reaches almost -90°. In this frequency range, the behavior of elastomer **E2** is predominantly capacitive, as the alternating field oscillates too fast for the ions to follow. The change of elastomer **E2** from resistive to capacitive behavior with increasing frequency is supported by the impedance plot as a function of frequency (Figure S12, Supporting Information). The large contribution of the ions to the capacitance in the sensors based on elastomer **E2** is proven by varying the frequency of the capacity measurement for one sensor (Figure 4b). The capacity change decreases when increasing the measurement frequency from 1 to 10 kHz and shows a further significant decrease when increasing the frequency to 100 kHz. The GF decreases to 9.5 for 10 kHz and to 1.7 for 100 kHz, where it is only slightly larger than the GF of the PDMS-based sensors

(0.41 ± 0.01). This is in accordance with the phase angle plot described above, where the elastomer changes from conductive behavior to capacitive behavior when increasing the frequency from 1 to 100 kHz.

The positive contribution of the tetramethylammonium ions to the sensor sensitivity can be described as follows. When a voltage is applied to measure the capacitance, these ions form an EDL at the interface between the electrode and elastomer **E2**. Upon stretching, the contact area between the electrode and core layer increases, which leads to an increase in capacitance. Due to its very low thickness, the capacitance of the EDL is much larger than the capacitance of the parallel plate capacitor, which causes a strong increase in sensitivity.

The sensitivity of our sensors with a GF of 12.7 ± 0.8 is significantly smaller compared to other supercapacitive sensors, e.g. Rao et al.^[17] reached a GF of 160. This is caused by the comparably low DC ionic conductivity of elastomer **E2** for which we determined a value of $(2.8 \pm 0.2) \times 10^{-7}$ S cm⁻¹. Ionic liquid and gel-based electrolytes show a much higher ionic conductivity of 10^{-2} – 10^{-4} S cm⁻¹ due to the higher ion mobility.^[39–41] However, EDL formation was previously still observed at even lower ionic conductivity values of 10^{-10} S cm⁻¹.^[42] The sensitivity of our sensors could be improved by increasing the ion concentration. In our case, increasing the concentration of TMAH is difficult, as it also serves as an initiator. A higher concentration would lead to shorter polymer chains, which increases the cross-linking density and decreases the elongation at break. In future work, additional ions could be added to the elastomer to increase the supercapacitive effect. Despite the lower sensitivity compared to other supercapacitive sensors, ions and polar side groups of the elastomer serve two functions in our material, increasing the capacity and enabling healing. The ions increase the capacity by forming an EDL and also enable healing by forming active silanolate end groups. The polar side groups also contribute to both effects by increasing the ion mobility on the one hand and enabling healing on the other hand by facilitating the backbiting of the active chain ends compared to non-polar silicone elastomers. Besides, many gel-based sensors suffer from freezing and leaking of the contained liquid, which impairs the electrical and mechanical stability of the sensors and can be overcome by applying an elastic solid-state electrolyte.^[43]

We tested the sensors' healing ability by cutting them with a blade and heating them to 75 °C for 10 min. Due to the thermoreversible nature of the elastomeric network, new bonds form across the cut upon cooling. The healed sensor can be stretched up to 40% without rupturing at the connecting site (Figure S13, Supporting Information). We tested the performance of the healed sensors by uniaxial stretching to 30%. The healed sensors perform similarly to the pristine sensors with a slightly larger normalized change in capacitance (Figure 4a). The sensor performance was also tested in cyclic tests. The sensors built from elastomer **E2** show a stable response without drift during 100 cycles (Figure 4c). The sensor can also be operated at higher frequencies, up to 0.5 Hz, with the same performance (Figure S14, Supporting Information). Even after healing, the sensor still works in cyclic tests and shows a stable response without drift after 100 cycles (Figure 4d). The healing of the electrode material was tested independently by measuring the resistance as a function of strain in the pristine state

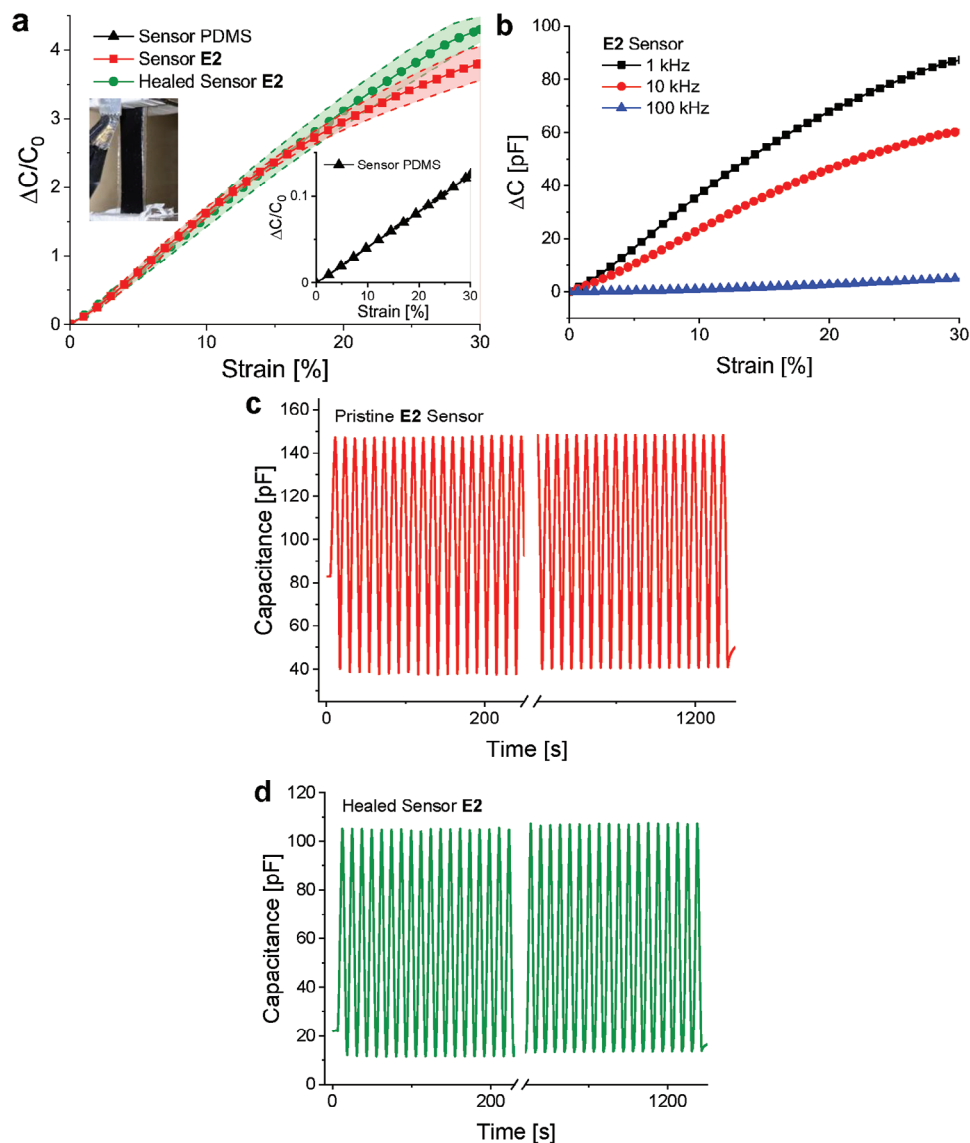


Figure 4. a) Normalized capacitance change as a function of strain for uniaxial stretching of sensors prepared from high-permittivity elastomer (E2) and PDMS. The sensors based on elastomer E2 recover their sensing property after cutting and healing at 75 °C for 10 min. b) Variation of the frequency of the capacity measurement for one sensor built from elastomer E2. The change in capacitance increases with decreasing frequency from 100 to 1 kHz. In this frequency range, elastomer E2 switches from capacitive to ion conductive behavior, which leads to an EDL at the interface between the electrode and elastomer E2. The capacity of this double layer is much larger than the capacity of the parallel plate capacitor, which is measured at high frequencies. c) Cyclic test of a sensor built from elastomer E2 with 100 cycles between 0% and 30% strain at 300 min⁻¹ (0.083 Hz). d) The same cyclic test was performed after cutting a sensor and healing at 75 °C for 10 min. The sensor shows a stable response without drift, even after healing.

and after cutting and healing by heating to 75 °C for 10 min (Figure S15, Supporting Information). Strains of 0–30% were applied in cyclic tests with frequencies of 1, 0.5, and 0.1 Hz. We observed a stable response of the resistance to strain over 10 cycles at different frequencies. After cutting and healing, the absolute values of the resistance are higher compared to the pristine state. This could be caused by insufficient healing of the percolated network of carbon black particles in the electrode material. The difference in resistance does not hinder the sensor from working but might require a new sensor calibration after the healing process.

4. 3D-Printing of Microstructured Core Layer and Integration in Soft Robotic Finger

Printing of soft sensors has become increasingly popular in the last few years.^[44–47] Printing allows the fabrication of customized sensor geometries with high shape flexibility, which could be applied in personalized medicine in the future.^[48] However, reported printed capacitive strain sensors suffer from low sensitivity with a maximum GF of 1.7.^[10,49] Printing electrode or core layer microstructures is especially interesting for supercapacitive sensors, as the change in the contact area

between the electrode and core layer upon deformation can be drastically increased.^[30–32] Many 3D-printing techniques intrinsically yield objects with a rough surface structure at the contact points between the printed lines. Alternatively, patterned structures with a larger distance between the lines can be printed.

The temperature-dependent rheology measurement of elastomer **E2** shows a thermoreversible softening of the material due to partial cleavage of the cross-links (Figure 3d). To determine the flow properties at elevated temperatures, we measured the viscosity and shear stress of elastomer **E2** as a function of the shear rate (flow curve) at 120 °C (Figure S9, Supporting Information). The material shows a Newtonian behavior with a linear relationship between shear rate and shear stress. The viscosity is independent of the shear rate. Even though elastomer **E2** does not show shear thinning, it can be printed by DIW at temperatures above 120 °C. The high viscosity of 100 Pa s avoids leaking of the material through the nozzle. After leaving the nozzle, the drop in temperature leads to a fast formation of the elastomer network, which prevents the flow of the printed structures. Three different structures were printed from elastomer **E2** through a nozzle with an inner diameter of 0.4 mm: lines (0°) in contact with each other, lines (0°) with a distance of 0.4 mm, and a grid (0°/90°) with a line distance of 0.4 mm. Schematic representations and optical microscopy images of a melt-pressed film and the three different printed structures are shown in Figure 5a. The images were taken from the printed film on top of an electrode film for better contrast. The melt-pressed film is isotropic without microstructure. The printed lines in contact with each other have a rough surface structure, due to the fabrication process of line-by-line printing. The lines and the grid with a 0.4 mm distance have air voids between the neighboring lines. Both show a symmetrical structure with only small defects, such as air bubbles in the grid structure.

We tested the sensors based on the 3D-printed structures in the same way as the melt-pressed sensors by uniaxial stretching to 30% strain in parallel direction to the printed lines while measuring the change in capacitance. The normalized change in capacitance is plotted in Figure 5b as a function of the strain for the melt-pressed sensor and two printed sensors. The sensitivity increases with increasing voids between the electrode and core layer (Table 2). It is larger for the sensor with printed lines in contact ($GF = 15.9 \pm 0.1$) compared to the melt-pressed sensor ($GF = 12.7 \pm 0.8$). The air in the small voids of the printed rough surface is pressed out at larger strains, increasing the contact area between the electrode and elastomer **E2**. This results in an additional gain in capacitance, as the area of the EDL is increased. Besides, the linearity is improved for the sensor with printed lines in contact ($R^2 = 0.998$) compared to the melt-pressed sensor ($R^2 = 0.995$). The sensor with printed lines with a 0.4 mm distance could not be measured successfully. The gap between the lines is too large and the electrodes can touch upon straining the sensor. To avoid contact between the electrodes, we printed a grid-like structure. The grid-like structure gives stability through additional lines perpendicular to the first layer and avoids any contact between the electrodes. The sensor with the grid-like structure exhibits a higher sensitivity ($GF = 17.7 \pm 0.2$) than the one with printed lines in contact ($GF = 15.9 \pm 0.1$) and excellent linearity of the response ($R^2 = 0.999$). Therefore, we increased the sen-

sitivity by $\approx 40\%$ by introducing a microstructure to the sensor core layer compared to the melt-pressed sensor. Unfortunately, the healing of the microstructured printed sensors is very difficult, as it is not feasible to bring the interfaces of all lines in good contact after cutting.

Soft strain sensors with healing ability are very interesting for application in damage-resilient soft robotics. The high sensitivity of our sensors at small strains of 0–30% is suitable for many soft robotic applications. One example is tracking the movement of a soft robotic gripper. As a proof of concept, we incorporated our sensor in a self-sensing soft robotic finger. A melt-pressed sensor from elastomer **E2** was attached to the back of a tendon-driven soft finger (Figure S16, Supporting Information). The finger was built from a self-healing elastomer based on a Diels–Alder system, which was already tested in previous studies on self-healing soft robots and is available on a larger scale.^[9] We attached the sensor to the back of the finger to measure the strain when bending the finger. The finger was bent repeatedly by pulling on a tendon attached to the fingertip. The displacement of the tendon follows a sinusoidal movement, which results in bending angles of the finger between 0° and 135°. In the meantime, the change in capacitance of the sensor was measured (Figure 5d; Video S1, Supporting Information). The bending angle was also measured by tracking the position of two red markers placed on the extremities of the finger with a camera. The bending angle and the capacitance signal are in good accordance, as shown in Figure S17 (Supporting Information). We reconstructed the bending angle from the capacitance signal by calculating a linear correlation between the measured bending angle and capacitance (Figure S18, Supporting Information). The reconstructed bending angle reflects the overall movement of the finger but still has errors, especially at lower bending angles. These errors can be caused by viscous losses of the sensor material or compression generated in the sensor at low bending angles (Figure 5c).

5. Conclusion

We have demonstrated supercapacitive strain sensors that show 30 times higher sensitivity than PDMS-based sensors and can heal by moderate heating to 75 °C for 10 min through siloxane equilibration. The high sensitivity of these supercapacitive sensors is enabled by the functional silicone elastomer core layer. It contains an active ionic initiator that can form an EDL at the interface with the electrodes, and polar nitrile side groups, which ensure sufficient ion mobility. The thermoreversible softening of the elastomers allows printing by DIW, which was used to prepare elastomer core layers with different infills. The sensors based on the printed core layers with partial infill show a higher sensitivity than the sensors with melt-pressed, isotropic core layer and linear response in a strain range of 0–30%. Finally, we demonstrated the integration of the sensors in a soft robotic finger, in which the reconstructed bending angle is in good accordance with the control measurement. In the future, this sensor technology could be used to print customized strain or pressure sensors with high sensitivity and linear response. The sensors can also be integrated into self-healing soft robotic devices to reach an integrally healable soft robot.

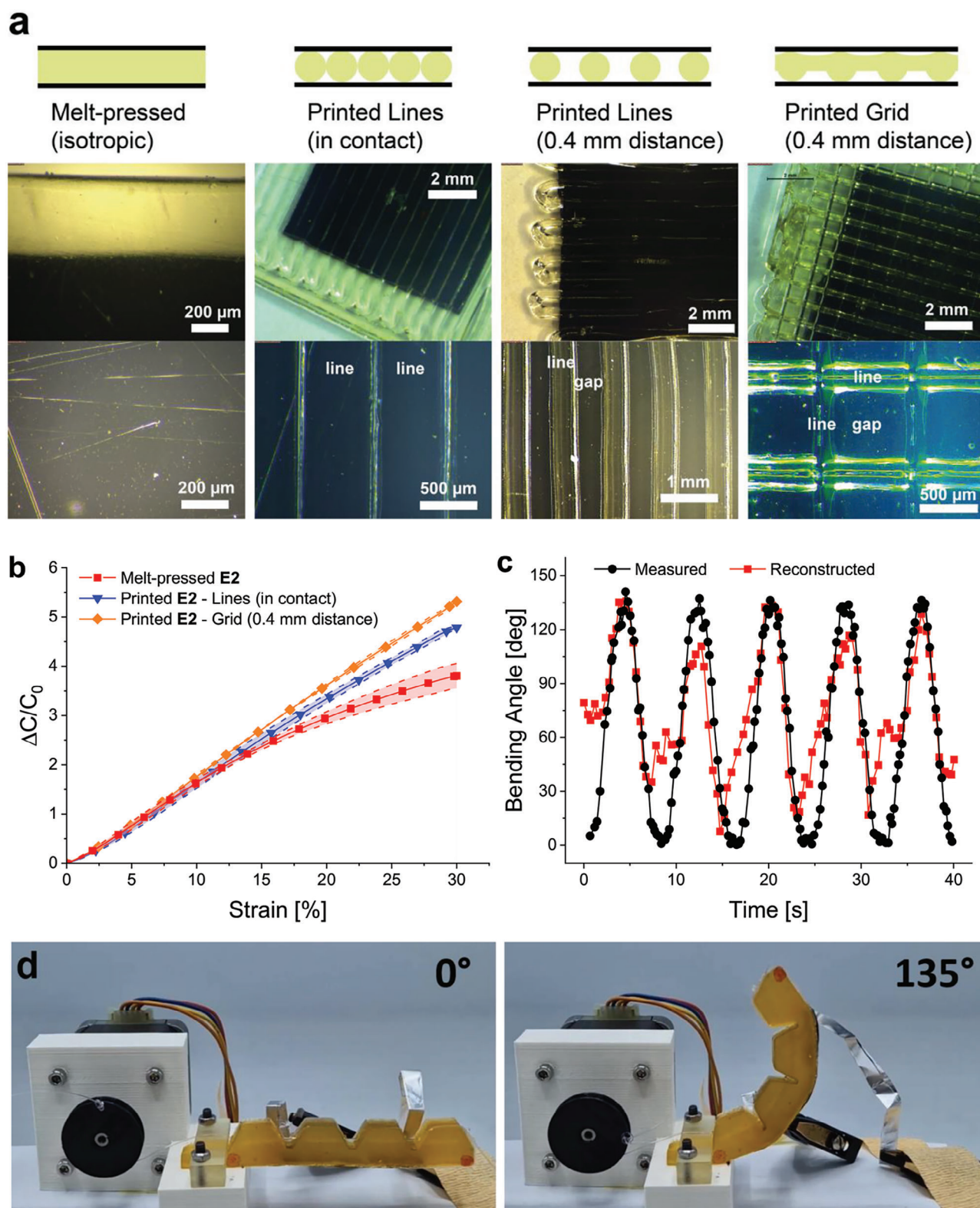


Figure 5. a) Schematic representation and optical microscope images of the printed structures of elastomer E2. b) Normalized change in capacitance for the printed sensors in comparison with the melt-pressed sensor. The sensor response increases with increasing air voids in the core layer toward higher strains. The sensor with printed lines with a 0.4 mm distance could not be measured successfully. c) Comparison of optically measured bending angle and bending angle reconstructed from the capacitance signal for a soft robotic finger equipped with a melt-pressed strain sensor. d) Soft robotic finger with an attached sensor at bending angles of 0° (left) and 135° (right).

Table 2. Performance of printed sensors in comparison with melt-pressed sensors.

Sensor	Gauge Factor	Linearity [R^2]
Melt-pressed	12.7 ± 0.8	0.995
Printed Lines (in contact)	15.9 ± 0.1	0.998
Printed Grid (0.4 mm distance)	17.7 ± 0.2	0.999

6. Experimental Section

More information about materials and characterizations, as well as the synthesis of monomer D_4^{CN} and cross-linker **PCL** can be found in Supporting Information.

Synthesis of the Healable Dielectric Elastomers: The respective amounts of monomer D_4^{CN} and cross-linker **PCL** were added to a 50 mL three-necked flask equipped with a magnetic stirrer. TMAH (0.92 mol% with respect to the polar monomer) was added as 25% solution in water and the water was removed in HV at RT for 30 min. Afterward, the flask was put under argon in a preheated oil bath at 110 °C, and the mixture was stirred for 10 min.

Synthesis of the Healable Electrode Material: Monomer D_4^{CN} (10.0 g, 19.7 mmol), cross-linker **PCL** (1.0 g, 1.0 mmol), and carbon black powder (1.94 g, 15 wt%) were mixed in the speed mixer for 5 min at 3000 rpm. TMAH (65 μ L, 0.92 mol% with respect to the polar monomer) was added as 25% solution in water and the mixture was mixed again for 5 min at 3000 rpm. The reaction mixture was poured on a glass substrate coated with Polytetrafluoroethylene (PTFE) foil and heated to 110 °C for 10 min on the heating plate.

Processing into Elastomer Thin Films: Elastomer films were prepared from the crude elastomers by melt pressing using a copper spacer with a thickness of 200 μ m between two poly(ethylene terephthalate) sheets coated with PTFE foil to yield films with a thickness of \approx 300 μ m. The arrangement was covered with metal plates on the top and bottom sides and placed inside a melt press. The temperature was set to 90 °C for the dielectric elastomer and 80 °C for the electrode material. After an equilibration time of 5 min, a pressure of 1000 kg was applied for 1 min. The resulting film was left to cool before removing it from the substrate. All characterization was carried out after waiting for at least 24 h.

Fabrication and Healable of Capacitive Strain Sensors: Films of elastomer **E2** were cut into strips of 3.5×1.2 cm² by die cutting. The electrode film was cut into strips of 3.3×0.8 cm². The film of elastomer **E2** was sandwiched between two films of electrode material and the assembly was heated to 70 °C for 5 min to merge the layers. For the healing experiments, the sensors were cut with a blade and then heated to 75 °C for 10 min on the heating plate. All characterization of the sensors was carried out after waiting for at least 24 h after heating. Sensors with PDMS (Ecoflex 30) as the core layer were fabricated accordingly, but without the heating steps.

3D-Printing of Microstructured Core Layers by DIW: Structured core layers were printed from elastomer **E2** by DIW using a printer from *Envision-TEC* (Bioplotter Manufacturing series). The elastomer was filled in a metal cartridge and extruded at a temperature of 120–130 °C and a pneumatic pressure of 7.3 bar through a nozzle with an inner diameter of 0.4 mm. The layer was printed onto a glass slide coated with PTFE film with a printing speed of 2–7 mm s⁻¹ to yield a dielectric layer with a thickness of \approx 300 μ m.

Fabrication of Sensors from Printed Core Layers: A strip of electrode film with a length of 2.5 cm and a width of 1.2 cm was placed on top of the printed core layer. The films are heated to 70 °C for 5 min on the heating plate. Afterward, the printed layer was cut around the electrode and the merged films were removed from the PTFE substrate. Microscope images were recorded from the film with the printed layer facing upward using a *Leica* MZ125 optical microscope with a *Leica* DMC2900 camera. Afterward, a second electrode film was placed on top of the printed layer and the films were again heated to 70 °C for 5 min. All characterizations were carried out after waiting for at least 24 h.

Sensor Integration in Soft Robotic Finger: A tendon-driven soft finger was prepared from a self-healing elastomer, according to the literature.^[9] A larger sensor with electrode dimensions of 4.8×0.8 cm² was prepared as described above and contacted with aluminum foil. The sensor was fixed to the back of the finger with Sil-Poxy glue from *Smooth-On*.

Supporting Information

Supporting Information is available from the Wiley Online Library or from the author.

Acknowledgements

The authors gratefully acknowledge the financial support from the EU Marie Curie ITN project SMART (860108), the European Research Council (ERC) under the European Union's Horizon 2020 research and innovation program (grant agreement No 101001182), the Swiss National Science Foundation (206021_150638/1). E.R., J.L., J.B., and S.T. gratefully acknowledge the Fond Wetenschappelijk Onderzoek (grant numbers 1S84120N, 12Y8622N, 12E1123N, and 1100416N). The authors also acknowledge D. Rentsch (Empa) for his support with the NMR measurements. D.M.O. thanks Prof. F. Nüesch (Empa) for the freedom to perform this research and Prof. J. Vermant (ETHZ) for manifold support.

Conflict of Interest

The authors declare no conflict of interest.

Data Availability Statement

The data that support the findings of this study are openly available in Zenodo at zenodo.org/records/8028154.

Keywords

3D-printing, high-permittivity elastomers, polar polysiloxanes, self-healing, soft robotics, supercapacitive strain sensors

Received: August 23, 2023

Revised: October 21, 2023

Published online: November 10, 2023

- [1] S.-T. Han, H. Peng, Q. Sun, S. Venkatesh, K.-S. Chung, S. C. Lau, Y. Zhou, V. A. L. Roy, *Adv. Mater.* **2017**, *29*, 1700375.
- [2] Y.-C. Lai, J. Deng, R. Liu, Y.-C. Hsiao, S. L. Zhang, W. Peng, H.-M. Wu, X. Wang, Z. L. Wang, *Adv. Mater.* **2018**, *30*, 1801114.
- [3] J. Shintake, Y. Piskarev, S. H. Jeong, D. Floreano, *Adv. Mater. Technol.* **2018**, *3*, 1700284.
- [4] T. Dong, Y. Gu, T. Liu, M. Pecht, *Sens. Actuator. A Phys.* **2021**, *326*, 112720.
- [5] A. J. Cheng, L. Wu, Z. Sha, W. Chang, D. Chu, C. H. Wang, S. Peng, *Adv. Mater. Technol.* **2023**, *8*, 2201959.
- [6] T. Cheng, X.-L. Yang, S. Yang, L. Li, Z.-T. Liu, J. Qu, C.-F. Meng, X.-C. Li, Y.-Z. Zhang, W.-Y. Lai, *Adv. Funct. Mater.* **2023**, *33*, 2210997.
- [7] B. Nie, X. Li, J. Shao, X. Li, H. Tian, D. Wang, Q. Zhang, B. Lu, *ACS Appl. Mater. Interfaces* **2017**, *9*, 40681.
- [8] X. Hu, F. Yang, M. Wu, Y. Sui, D. Guo, M. Li, Z. Kang, J. Sun, J. Liu, *Adv. Mater. Technol.* **2022**, *7*, 2100769.

- [9] E. Roels, S. Terryn, J. Brancart, F. Sahræeazartamar, F. Clemens, G. Van Assche, B. Vanderborght, *Mater. Today Electron.* **2022**, *1*, 100003.
- [10] H. Liu, H. Zhang, W. Han, H. Lin, R. Li, J. Zhu, W. Huang, *Adv. Mater.* **2021**, *33*, 8.
- [11] S. Terryn, J. Langenbach, E. Roels, J. Brancart, C. Bakkali-Hassani, Q.-A. Poutrel, A. Georgopoulou, T. George Thuruthel, A. Safaei, P. Ferrentino, T. Sebastian, S. Norvez, F. Iida, A. W. Bosman, F. Tournilhac, F. Clemens, G. Van Assche, B. Vanderborght, *Mater. Today* **2021**, *47*, 187.
- [12] M. Khatib, O. Zohar, H. Haick, *Adv. Mater.* **2021**, *33*, 2101498.
- [13] J. Zhang, L. Wan, Y. Gao, X. Fang, T. Lu, L. Pan, F. Xuan, *Adv. Electron. Mater.* **2019**, *5*, 1900285.
- [14] X. Jing, H. Li, H.-Y. Mi, Y.-J. Liu, P.-Y. Feng, Y.-M. Tan, L.-S. Turng, *Sens. Actuator. B Chem.* **2019**, *295*, 159.
- [15] Q. Zhang, S. Niu, L. Wang, J. Lopez, S. Chen, Y. Cai, R. Du, Y. Liu, J.-C. Lai, L. Liu, C.-H. Li, X. Yan, C. Liu, J. B.-H. Tok, X. Jia, Z. Bao, *Adv. Mater.* **2018**, *30*, 1801435.
- [16] L. Ling, F. Liu, J. Li, G. Zhang, R. Sun, C.-P. Wong, *Macromol. Chem. Phys.* **2019**, *219*, 1800369.
- [17] V. K. Rao, N. Shauloff, X. Sui, H. D. Wagner, R. Jelinek, *J. Mater. Chem. C* **2020**, *8*, 6034.
- [18] G. Yang, K. Zhu, W. Guo, D. Wu, X. Quan, X. Huang, S. Liu, Y. Li, H. Fang, Y. Qiu, Q. Zheng, M. Zhu, J. Huang, Z. Zeng, Z. Yin, H. Wu, *Adv. Funct. Mater.* **2022**, *32*, 29.
- [19] R. B. Mishra, N. El-Atab, A. M. Hussain, M. M. Hussain, *Adv. Mater. Technol.* **2021**, *6*, 2001023.
- [20] S. Wu, S. Peng, Y. Yu, C.-H. Wang, *Adv. Mater. Technol.* **2020**, *5*, 1900908.
- [21] A. Chortos, J. Liu, Z. Bao, *Nat. Mater.* **2016**, *15*, 937.
- [22] X. Liu, H. Sun, S. Liu, Y. Jiang, Z. Yin, B. Yu, N. Ning, M. Tian, L. Zhang, *Compos. Part B Eng.* **2021**, *223*, 109103.
- [23] S.-Y. Liu, J.-G. Lu, H.-P. D. Shieh, *IEEE Sens. J.* **2018**, *18*, 1870.
- [24] J. Choi, D. Kwon, K. Kim, J. Park, D. D. Orbe, J. Gu, J. Ahn, I. Cho, Y. Jeong, Y. Oh, I. Park, *ACS Appl. Mater. Interfaces* **2020**, *12*, 1698.
- [25] J. Qin, L.-J. Yin, Y.-N. Hao, S.-L. Zhong, D.-L. Zhang, K. Bi, Y.-X. Zhang, Y. Zhao, Z.-M. Dang, *Adv. Mater.* **2021**, *33*, 2008267.
- [26] V. Amoli, J. S. Kim, S. Y. Kim, J. Koo, Y. S. Chung, H. Choi, D. H. Kim, *Adv. Funct. Mater.* **2020**, *30*, 1904532.
- [27] B. Nie, R. Li, J. Cao, J. D. Brandt, T. Pan, *Adv. Mater.* **2015**, *27*, 6055.
- [28] Y. Qin, X. Zhang, A. Zheng, Q. Xia, *Adv. Mater. Technol.* **2022**, *7*, 2100510.
- [29] N. Bai, L. Wang, Q. Wang, J. Deng, Y. Wang, P. Lu, J. Huang, G. Li, Y. Zhang, J. Yang, K. Xie, X. Zhao, C. F. Guo, *Nat. Commun.* **2020**, *11*, 3.
- [30] A. Chhetry, J. Kim, H. Yoon, J. Y. Park, *ACS Appl. Mater. Interfaces* **2019**, *11*, 3438.
- [31] Q. Su, Q. Zou, Y. Li, Y. Chen, S. Y. Teng, J. T. Kelleher, R. Nith, P. Cheng, N. Li, W. Liu, S. Dai, Y. Liu, A. Mazursky, J. Xu, L. Jin, P. Lopes, S. Wang, *Sci. Adv.* **2021**, *7*, 48.
- [32] M.-J. Yin, Z. Yin, Y. Zhang, Q. Zheng, A. P. Zhang, *Nano Energy* **2019**, *58*, 96.
- [33] P. Zheng, T. J. McCarthy, *J. Am. Chem. Soc.* **2012**, *134*, 2024.
- [34] J. Von Szczepanski, P. M. Danner, D. M. Opris, *Adv. Sci.* **2022**, *9*, 2202153.
- [35] A. Jourdain, R. Asbai, O. Anaya, M. M. Chehimi, E. Drockenmuller, D. Montarnal, *ACS Appl. Mater. Interfaces* **2020**, *53*, 6.
- [36] X. Kuang, G. Liu, X. Dong, D. Wang, *Mater. Chem. Front.* **2017**, *1*, 111.
- [37] G. Scheltjens, M. M. Diaz, J. Brancart, G. Van Assche, B. Van Mele, *React. Funct. Polym.* **2013**, *73*, 413.
- [38] R. J. Sheridan, C. N. Bowman, *Macromolecules* **2012**, *45*, 7634.
- [39] S. H. Kim, K. Hong, W. Xie, K. H. Lee, S. Zhang, T. P. Lodge, C. D. Frisbie, *Adv. Mater.* **2013**, *25*, 1822.
- [40] J. H. Cho, J. Lee, Y. He, B. S. Kim, T. P. Lodge, C. D. Frisbie, *Adv. Mater.* **2008**, *20*, 686.
- [41] M. Armand, F. Endres, D. R. Macfarlane, H. Ohno, B. Scrosati, *Nat. Mater.* **2009**, *8*, 621.
- [42] D. Kong, R. Pfattner, A. Chortos, C. Lu, A. C. Hinckley, C. Wang, W.-Y. Lee, J. W. Chung, Z. Bao, *Adv. Funct. Mater.* **2016**, *26*, 4680.
- [43] C. Zhang, H. Zheng, J. Sun, Y. Zhou, W. Xu, Y. Dai, J. Mo, Z. Wang, *Adv. Mater.* **2022**, *34*, 2105996.
- [44] A. Frutiger, J. T. Muth, D. M. Vogt, Y. Mengüç, A. Campo, A. D. Valentine, C. J. Walsh, J. A. Lewis, *Adv. Mater.* **2015**, *27*, 2440.
- [45] X.-Y. Yin, Y. Zhang, J. Xiao, C. Moorlag, J. Yang, *Adv. Funct. Mater.* **2019**, *29*, 1904716.
- [46] K. Li, H. Wei, W. Liu, H. Meng, P. Zhang, C. Yan, *Nanotechnology* **2018**, *29*, 185501.
- [47] Z. Lei, Q. Wang, P. Wu, *Mater. Horiz.* **2017**, *4*, 694.
- [48] T. Q. Trung, N.-E. Lee, *Adv. Mater.* **2016**, *28*, 4338.
- [49] E. Cholleti, J. Stringer, M. Assadian, V. Battmann, C. Bowen, K. Aw, *Sensors* **2019**, *19*, 42.